A&A 444, 403–415 (2005)
DOI: 10.1051/0004-6361:20053613

Astronomy & Astrophysics

High energy γ-ray emission from the starburst nucleus of NGC 253⋆

E. Domingo-Santamaría[1] and D. F. Torres[2,1]

[1] Institut de Física d'Altes Energies (IFAE), Edifici C-n, Campus UAB, 08193 Bellaterra, Spain
[2] Lawrence Livermore National Laboratory, 7000 East Avenue, L-413, Livermore, CA 94550, USA

Received 10 June 2005 / Accepted 9 August 2005

ABSTRACT

Both the high density medium that characterizes the central regions of starburst galaxies and its power to accelerate particles up to relativistic energies make these objects good candidates for γ-ray sources. In this paper we present a self-consistent model of the multifrequency emission of the starburst galaxy NGC 253 from radio to γ-rays. The model agrees with all current measurements and provides predictions for the high energy behavior of the NGC 253 central region. In particular, we discuss prospects for observations with the HESS array (and comparison with their recently obtained data) and GLAST satellite.

Key words. ISM: cosmic rays – galaxies: starburst – galaxies: individual: NGC 253

1. Introduction

Starburst galaxies (and star-forming regions in general) are expected to be detected as γ-ray sources. They have both a large amount of target material and multiple shocks to accelerate particles up to relativistic energies, due to the presence of supernova remnants and the powerful stellar winds of their numerous young stars. Pion decay production of γ-rays, usually dominant under such conditions, is thought to produce significant γ-ray fluxes.

Approximately 90% of the high-energy γ-ray luminosity of the Milky Way ($\sim$1.3 $\times 10^6$ $L_\odot$, Strong et al. 2000) is diffuse emission from cosmic ray interactions with interstellar gas and photons (Hunter et al. 1997). However, the LMC is the only external galaxy that has been detected in its diffuse γ-ray emission (Sreekumar et al. 1992), a fact explained by the isotropic flux dilution by distance. At 1 Mpc, for example, the flux of the Milky Way would be approximately 2.5×10^{-8} photons cm^{-2} s^{-1} (>100 MeV), which is below the sensitivity achieved up to now in the relevant energy domain. The Energetic γ-ray Experiment, EGRET, did not detect any starburst. Upper limits were imposed for M 82, $F(E > 100\ \mathrm{MeV}) < 4.4 \times 10^{-8}$ photons cm^{-2} s^{-1}, and NGC 253, $F(E > 100\ \mathrm{MeV}) < 3.4 \times 10^{-8}$ photons cm^{-2} s^{-1} (Blom et al. 1999), the two nearest starbursts, as well as for many luminous infrared galaxies, for which similar constraints were found (Torres et al. 2004a). These upper limits are barely above the theoretical predictions of models for the γ-ray emission of galaxies, constructed with different levels of detail (see Torres 2004b for a review). Starbursts and luminous infrared galaxies are expected to compensate for the flux dilution produced by their relatively larger distance to Earth with their higher cosmic ray flux, and become sources for the next generation of instruments measuring photons in the 100 MeV–10 GeV regime, like the Gamma-ray Large Area Telescope, GLAST (e.g., Völk et al. 1996; Paglione et al. 1996; Blom et al. 1999; Torres et al. 2004; Torres 2004).

In this paper, we analyze one such galaxy, the well-studied starburst NGC 253. We present a self-consistent multiwavelength modelling of the central region of the galaxy, taking into account the latest measurements of densities, supernova explosion rate, radio emission, and molecular mass, among other physical parameters that we use as input for our scenario.

2. CANGAROO observations of NGC 253

Recently, the CANGAROO collaboration reported detection of NGC 253 at TeV γ-ray energies (an 11σ confidence level claim), observed during a period of two years in 2000 and 2001 for about 150 h (Itoh et al. 2002, 2003). Their measured differential flux was fitted by Itoh et al. (2003) with a power law and an exponential cutoff, obtaining

$$\frac{\mathrm{d}F}{\mathrm{d}E} = (2.85 \pm 0.71) \times 10^{-12} \times (E/1\ \mathrm{TeV})^{(-3.85\pm0.46)}\ \mathrm{cm}^{-2}\,\mathrm{s}^{-1}\,\mathrm{TeV}^{-1},$$

and

$$\frac{\mathrm{d}F}{\mathrm{d}E} = a\mathrm{e}^{\sqrt{E_0}/b}(E/E_0)^{-1.5}\mathrm{e}^{-\sqrt{E}/b}\ \mathrm{cm}^{-2}\,\mathrm{s}^{-1}\,\mathrm{TeV}^{-1},$$

⋆ Appendix is only available in electronic form at http://www.edpsciences.org

with $a = 6 \times 10^{-5}$ cm^{-2} s^{-1} TeV^{-1}, $E_0 = 0.0002$ TeV, and $b = 0.25 \pm 0.01$ $\sqrt{\text{TeV}}$. Both parameterizations are reasonable reproductions of the observational data, although the former is clearly preferred for simplicity given an equally good fit. The flux uncertainty is the square root of the quadratic sum of the statistical and systematic errors. Note that the slope of the power law spectrum is very uncertain, but steep. Indeed, an extrapolation of this power-law spectrum to lower energies violates the measured upper limits in the GeV regime. The CANGAROO collaboration suggested a turn-over below the TeV region and proposed the second spectral form. They also claimed that the emission at the highest energies is inconsistent with it being produced in a point-like source, and instead proposed an inverse Compton origin for it in a kpc-scale γ-ray halo.

The HESS array has also observed NGC 253 (see below). In several other observations of sources that have previously been targets for CANGAROO, the HESS collaboration has presented results in clear contradiction to the former CANGAROO reports. This is most notably the case for SN 1006 (Aharonian et al. 2005a), PSR B1706-44 (Aharonian et al. 2005b), also for the supernova remnant RX J1713-3857 to some extent (Aharonian et al. 2004a), and the Galactic Center (Aharonian et al. 2004b). This may suggest some kind of systematic difference in the treatment of both sets of observational data. Such a systematic effect should explain why CANGAROO spectra are steeper and why their measured fluxes are one order of magnitude higher than the upper limits or measurements obtained with HESS. The CANGAROO collaboration is now calibrating their stereo system and will be re-observing these problematic cases within a year or so (R. Enomoto 2005, private communication).

In what follows, we focus on producing a detailed multiwavelength theoretical model for the central region of NGC 253, irrespective of CANGAROO measurements; i.e., we will not try to reproduce their spectrum, but will derive predictions of fluxes based on a set of well-founded assumptions. The aim is to see whether a model based on observations at all wavelengths and first principles would –while consistent with multiwavelength testing– predict that the central region of NGC 253 alone can produce a sufficiently high γ-ray flux to be detected by the current ground-based Cerenkov telescopes and future MeV–GeV satellites. The central region of the galaxy would look like a point-like source for the field of view and angular resolution of imaging Cerenkov telescopes. Therefore, we will be able to answer if one can expect a HESS non-confirmation of CANGAROO results regarding perhaps both the flux and the extension.

3. Phenomenology of the central region of NGC 253

A wealth of new multiwavelength data was obtained for NGC 253 during the last decade, after the previous modelling by Paglione et al. (1996), which did not include photons energies above 100 GeV (see below). It is located at a distance of ~2.5 Mpc (Turner & Ho 1985; Maurbersger et al. 1996) and is a nearly edge-on (inclination 78°, Pence 1981) barred Sc galaxy. The continuum spectrum of NGC 253 peaks in the FIR at about 100 μm with a luminosity of 4×10^{10} $L_\odot$ (Telesco & Harper 1980; Rice et al. 1988; Melo et al. 2002). The FIR luminosity is at least a factor of 2 larger than that of our own Galaxy (Cox & Mezger 1989; Dudley & Wynn-Williams 1999), and it mainly comes from the central nucleus, about half of it according to the Melo et al. (2002) 1 arcmin resolution ISOPHOT observations. IR emission can be understood as cold ($T \sim 50$ K) dust reprocessing of stellar photon fields.

When observed at 1 pc resolution, at least 64 individual compact radio sources have been detected within the central 200 pc of the galaxy (Ulvestad & Antonucci 1997), and roughly 15 of them are within the central arcsec of the strongest radio source, considered to be either a buried active nucleus or a very compact SNR. Of the strongest 17 sources, about one half have flat spectra and half have steep spectra. This indicates that perhaps half of the individual radio sources are dominated by thermal emission from H II regions, and half are optically thin synchrotron sources, presumably SNRs. There is no compelling evidence of any sort of variability in any of the compact sources over an 8-yr time baseline. The most powerful flat-spectrum central radio source is clearly resolved in the study of Ulvestad & Antonucci (1997) and appears to be larger than the R136 cluster located in 30 Doradus, containing about 10^5 $M_\odot$ in stars and 600 $M_\odot$ in ionized gas. The age was estimated to be less than 4×10^6 yr. The region surrounding the central 200 pc has also been observed with subarcsec resolution and 22 additional radio sources stronger than 0.4 mJy were detected within 2 kpc of the galaxy nucleus (Ulvestad 2000). The region outside the central starburst may account for about 20% of the star formation of NGC 253, is subject to a supernova explosion rate well below 0.1 yr^{-1}, and has an average gas density in the range 20–200 cm^{-3}, much less than in the most active nuclear region of NGC 253 (Ulvestad 2000).

Carilli (1996) presented low frequency radio continuum observations of the nucleus at high spatial resolution. Free-free absorption was claimed as the mechanism producing a flattening of the synchrotron curve at low energies, with a turnover frequency located between $10^{8.5}$ and 10^9 Hz. The emission measures needed for this turnover to happen is at least 10^5 pc cm^{-6} for temperatures on the order of 10^4 K. Tingay (2004) observed NGC 253 using the Australian Long Baseline Array and provided fits with free-free absorption models for the radio spectrum of six sources. He concluded that the free-free opacity in the central region has to be in the range of 1 to 4 at 1.4 GHz, implying emission measures of a few times 10^6 pc cm^{-6} in this particular direction, again for temperatures of the order of 10^4 K.

As shown by infrared, millimeter, and centimeter observations, the 200 pc central region dominates the current star formation in NGC 253, and is considered as the starburst central nucleus (e.g., Ulvestad & Antonucci 1997; Ulvestad 2000). Centimeter imaging of this inner starburst and the limits on variability of radio sources indicate a supernova rate less than 0.3 yr^{-1} (Ulvestad & Antonucci 1997), which is consistent with results ranging from 0.1 to 0.3 yr^{-1} inferred from models of the infrared emission of the entire galaxy (Rieke et al. 1980, 1988; Forbes et al. 1993). Van Buren & Greenhouse (1994)

developed a direct relationship between the FIR luminosity and the rate of supernova explosions, starting from Chevalier's (1982) model for radio emission from supernovae blast waves expanding into the ejecta of their precursor stars. The result is $\mathcal{R} = 2.3 \times 10^{-12} L_{\rm FIR}/L_\odot$ yr^{-1}, which is in agreement with the previous estimates within uncertainties. The star formation rate at the central region has been computed from IR observations, resulting in 3.5 $M_\odot\,{\rm yr}^{-1}$, and it represents about 70% of the total star formation rate measured for NGC 253 (Melo et al. 2002). When compared with Local Group Galaxies, the supernova rate in NGC 253 is one order of magnitude larger than that of M 31, the largest of the Local Group (Pavlidou & Fields 2001).

Paglione et al. (2004) obtained high resolution ($5\farcs2 \times 5\farcs2$) interferometric observations of the CO line $J = 1 \rightarrow 0$ in order to study the structure and kinematics of the molecular gas in the central nucleus. This study enhances that of Sorai et al. (2000), which obtained compatible results, although done with less angular resolution. The general morphology of the CO map is consistent with other high resolution studies. It shows an extended ridge of emission aligned with an infrared-bright bar and a central group of bright clouds aligned with the major axis of the galaxy, orbiting the radio nucleus in a possible ring. The central clouds move around the radio nucleus as a solid body, similar to the distribution of the radio sources, central HCN clouds, and central near-infrared emission (Paglione et al. 1995, 1997; Ulvestad & Antonucci 1997). Much of the molecular gas in NGC 253 appears to be highly excited (Wild et al. 1992; Mao et al. 2000; Ward et al. 2003). Observations of $J = 4 \rightarrow 3$ and $J = 6 \rightarrow 5$ transitions of CO, as well as HCN lines, suggest the existence of localized spots with values of densities in excess of 10^4 cm^{-3} (Israel & Baas 2002; Paglione et al. 1997, 1995; Harris et al. 1991). Bradford et al. (2003) report CO $J = 7 \rightarrow 6$ observations and also find that the bulk of molecular gas in the central 180 pc of the galaxy is highly excited and at a temperature of about 120 K. They conclude that the best mechanism for heating the gas is cosmic ray bombardment over the gas residing in clouds, with density about 4.5×10^4 cm^{-3}.

Current estimates of the gas mass in the central 20″–50″ (<600 pc) region range from 2.5×10^7 $M_\odot$ (Harrison et al. 1999) to 4.8×10^8 $M_\odot$ (Houghton et al. 1997); see Bradford et al. (2003), Sorai et al. (2000), and Engelbracht et al. (1998) for discussions. For example, using the standard CO to gas mass conversion, the central molecular mass was estimated as 1.8×10^8 $M_\odot$ (Mauersberger et al. 1996). It would be factor of ∼3 lower if such is the correction to the conversion factor in starburst regions, which are better described as a filled intercloud medium, as in the case of ULIRGs, instead of a collection of separate large molecular clouds; see Solomon et al. (1997), Downes & Solomon (1998), and Bryant & Scoville (1999) for discussions. Thus we will assume, in agreement with the mentioned measurements, that within the central 200 pc, a disk of 70 pc height has $\sim 2 \times 10^7$ $M_\odot$ uniformly distributed, with a density of ∼600 cm^{-3}. Additional target gas mass with an average density of ∼50 cm^{-3} is assumed to populate the central kpc outside the innermost region, but subject to a smaller supernova explosion rate ∼0.01 yr^{-1}, 10% of that found in the most powerful nucleus (Ulvestad 2000).

The central region of this starburst is packed with massive stars. Watson et al. (1996) discovered four young globular clusters near the center of NGC 253; they alone can account for a mass well in excess of 1.5×10^6 $M_\odot$ (see also Keto et al. 1999). Assuming that the star formation rate has been continuous in the central region for the past 10^9 yrs and a Salpeter IMF for 0.08–100 $M_\odot$, Watson et al. (1996) find that the bolometric luminosity of NGC 253 is consistent with 1.5×10^8 $M_\odot$ of young stars. Physical, morphological, and kinematic evidence for the existence of a galactic superwind has been found for NGC 253 (e.g., McCarthy et al. 1987; Heckman et al. 1990; Strickland et al. 2000, 2002; Pietsch et al. 2001; Forbes et al. 2000; Weaver et al. 2002; Sugai et al. 2003). This superwind creates a cavity of hot (∼10^8 K) gas, with longer cooling times than the typical expansion timescales. As the cavity expands, a strong shock front is formed on the contact surface with the cool interstellar medium. Shock interactions with low and high density clouds can produce X-ray continuum and optical line emission, respectively, both of which have been directly observed (McCarthy et al. 1987). The shock velocity can reach thousands of km s^{-1}. This wind has been proposed as the convector of particles that have been already accelerated in individual SNRs, to the larger superwind region, where Fermi processes could upgrade their energy up to that detected in ultra high energy cosmic rays (Anchordoqui et al. 1999; Anchordoqui et al. 2003; Torres & Anchordoqui 2004).

4. Diffuse modelling

The approach to compute the steady multiwavelength emission from NGC 253 follows the one implemented in *Q*-DIFFUSE, which we have already used, but with some further improvements (Torres 2004). The steady state particle distribution is computed within *Q*-DIFFUSE as the result of an injection distribution being subject to losses and secondary production in the ISM. In general, the injection distribution may be defined to a lesser degree of uncertainty when compared with the steady state one, since the former can be directly linked to observations. The injection proton emissivity, following Bell (1978), is assumed to be a power law in proton kinetic energies, with index p, $Q_{\rm inj}(E_{\rm p,kin}) = K(E_{\rm p,kin}/{\rm GeV})^{-p}$, where K is a normalization constant and units are such that $[Q] = {\rm GeV}^{-1}\ {\rm cm}^{-3}\ {\rm s}^{-1}$. The normalization K is obtained from the total power transferred by supernovae into CRs kinetic energy within a given volume $\int_{E_{\rm p,kin,min}}^{E_{\rm p,kin,max}} Q_{\rm inj}(E_{\rm p,kin}) E_{\rm p,kin} {\rm d}E_{\rm p,kin} = -K E_{\rm p,kin,min}^{-p+2}/(-p+2) \equiv \sum_i \eta_i \mathcal{P} \mathcal{R}_i / V$ where it was assumed that $p \neq 2$ and we used the fact that $E_{\rm p,kin\,min} \ll E_{\rm p,kin,max}$ in the second equality. The expression $\mathcal{R}_i$ ($\sum_i \mathcal{R}_i = \mathcal{R}$) is defined as the rate of supernova explosions in the star-forming region being considered, with V its volume and η_i the transferred fraction of the supernova explosion power ($\mathcal{P} \sim 10^{51}$ erg) into CRs (e.g., Torres et al. 2003 and references therein). The summation over i takes into account that not all supernovae will transfer the same amount of power into CRs (alternatively, that not all supernovae will release the same power). The rate of power transfer is assumed

to be in the range $0.05 \lesssim \eta_i \lesssim 0.15$, and the average value for η is $\sim$10%. At low energies, the distribution of cosmic rays is flatter; e.g., it would be given by Eq. (6) of Bell (1978), correspondingly normalized. We numerically verified that to neglect this difference at low energy does not produce any important change in the computation of secondaries, and especially on γ-rays at the energies of interest.

The general diffusion-loss equation is given by (see, e.g., Longair 1994, p. 279; Ginzburg & Syrovatskii 1964, p. 296)

$$-D\,\nabla^2 N(E) + \frac{N(E)}{\tau(E)} - \frac{\mathrm{d}}{\mathrm{d}E}\left[b(E)N(E)\right] - Q(E) = -\frac{\partial N(E)}{\partial t}\cdot \quad (1)$$

In this equation, D is the scalar diffusion coefficient, $Q(E)$ represents the source term appropriate to the production of particles with energy E, $\tau(E)$ stands for the confinement timescale, $N(E)$ is the distribution of particles with energies in the range E and $E + \mathrm{d}E$ per unit volume, and $b(E) = -(\mathrm{d}E/\mathrm{d}t)$ is the rate of loss of energy. The functions $b(E)$, $\tau(E)$, and $Q(E)$ depend on the kind of particles. In the steady state, $\partial N(E)/\partial t = 0$, and, under the assumption of a homogeneous distribution of sources, the spatial dependence is considered to be irrelevant, so that $D\,\nabla^2 N(E) = 0$. Equation (1) can be solved by using the Green function

$$G(E, E') = \frac{1}{b(E)} \exp\left(-\int_E^{E'} \mathrm{d}y \frac{1}{\tau(y)b(y)}\right), \quad (2)$$

such that for any given source function, or emissivity, $Q(E)$, the solution is

$$N(E) = \int_E^{E_{\max}} \mathrm{d}E' Q(E') G(E, E'). \quad (3)$$

The confinement timescale will be determined by several contributions. One on hand, we consider the characteristic escape time in the homogeneous diffusion model (Berezinskii et al. 1990, p. 50–52 and 78) $\tau_D = R^2/(2D(E)) = \tau_0/(\beta(E/\mathrm{GeV})^\mu)$, where β is the velocity of the particle in units of c, R is the spatial extent of the region from where particles diffuse away, and $D(E)$ is the energy-dependent diffusion coefficient, whose dependence is assumed $\propto E^\mu$, with $\mu \sim 0.5$[1]. τ_0 is the characteristic diffusive escape time at $\sim$1 GeV. It is not known for NGC 253, one can only assume its value and compare it with the one for other galaxies (e.g. our own Galaxy, or M 33, Duric et al. 1995); the value we choose also parallels the one obtained in an earlier study of NGC 253 or on M 82 (Paglione et al. 1996; Blom et al. 1999). We analyze the sensitivity of the model to τ_0 below. On the other, the total escape timescale will also take into account that particles can be carried away by the collective effect of stellar winds and supernovae. The convective timescale, τ_c, is $\sim R/V$, where V is the collective wind velocity. For a wind velocity of 300 km s^{-1} and a radius of about the size of the innermost starburst (see below), this timescale is less than a million years (3×10^5 yr). The outflow velocity is not very well known; however, minimum reasonable values between 300 and 600 km s^{-1} have been claimed, and could even reach values on the order of thousands of km s^{-1} (Strickland et al. 2002). Pion losses (which are catastrophic, since the inelasticity of the collision is about 50%) produce a loss timescale $\tau_{\mathrm{pp}}^{-1} = (\mathrm{d}E/\mathrm{d}t)^{\mathrm{pion}}/E$ (see, e.g., Mannheim & Schlickeiser 1994), which is similar in magnitude to the convective timescale and dominates with it the shaping of the proton spectrum. Thus, in general, for energies higher than the pion production threshold, $\tau^{-1}(E) = \tau_{\mathrm{D}}^{-1} + \tau_{\mathrm{c}}{}^{-1} + \tau_{\mathrm{pp}}^{-1}$. For electrons, the total rate of energy loss considered is given by the sum of that involving ionization, inverse Compton scattering, bremsstrahlung, and synchrotron radiation. We also incorporated adiabatic losses. A full Klein-Nishina cross section is used while computing photon emission, and either Thomson or extreme Klein-Nishina approximations, as needed, are used while computing losses. For the production of secondary electrons, *Q*-DIFFUSE computes knock-on electrons and charged pion processes producing both electrons and positrons. In the case of γ-ray photons, we compute bremsstrahlung, inverse Compton and neutral pion decay processes. For the latter, an Appendix provides a more detailed discussion of the different approaches to compute the neutral pion-induced γ-ray emissivity. For radio photons, we compute the synchrotron and free-free emission using the steady distribution of electrons. Free-free absorption is also considered in order to reproduce the radio data at low frequencies. The FIR emission is modelled with a dust emissivity law given by $\nu^\sigma B(\epsilon, T)$, where $\sigma = 1.5$ and B is the Planck function. The computed FIR photon density is used as a target for inverse Compton process as well as to account for losses in the γ-ray scape. The latter basically comes from the opacity to $\gamma\gamma$ pair production with the photon field of the galaxy nucleus. The fact that the dust within the starburst reprocesses the UV star radiation to the less energetic infrared photons implies that the opacity to $\gamma\gamma$ process is significant only at the highest energies. The opacity to pair production from the interaction of a γ-ray photon in the presence of a nucleus of charge Z is considered, too. For further details and relevant formulae see Torres (2004).

4.1. Comparison with previous models

When compared with the previous study of high energy emission from NGC 253 by Paglione et al. (1996), several methodological and modelling differences need to be mentioned. The distance, size, gas mass, density, and supernova explosion rate of the central region that they assume are different from those quoted in Table 1. Based on earlier data (e.g., Canzian et al. 1988), the former authors modelled a starburst region at 3.4 Mpc (a factor of 1.36 farther than the one currently adopted), with a 325 pc radius (about 3 times larger than the one adopted here). This region is larger than implied by current knowledge of the central starburst, where the supernova explosion rate Paglione et al. used is actually found and the cosmic ray density is maximally enhanced. The average density assumed by Paglione et al., 300 cm^{-3}, gives a target mass $\sim 2 \times 10^8\ M_\odot$, which is at the upper end of all current claims

[1] We emphasize that the use of a homogeneous model is an assumption, but is justified in the compactness of the innermost starburst region. We are basically assuming that there is a homogeneous distribution of supernovae in the central hundreds of pc, which is supported observationally (Ulvestad & Antonucci 1997).

Table 1. Measured, assumed, and derived values for different physical quantities at the innermost starburst region of NGC 253 (IS), a cylindrical disk with height 70 pc, and its surrounding disk (SD).

Physical parameters	Symbol	Value	Units	Comment
Distance	D	2.5	Mpc	ST
Inclination	i	78	degrees	ST
Infrared Luminosity of the innermost starburst (IS)	$L_{\rm IR}$	2×10^{10}	$L_\odot$	ST
Radius of the IS	–	100	pc	ST
Radius surrounding disk (SD)	–	1000	pc	ST
Uniform density of the IS	$n_{\rm IS}$	~600	cm^{-3}	ST
Uniform density of the SD	$n_{\rm SD}$	~50	cm^{-3}	ST
Gas mass of the IS	$M_{\rm IS}$	$\sim 3 \times 10^7$	$M_\odot$	ST
Gas mass of the SD	$M_{\rm SD}$	$\sim 2.5 \times 10^8$	$M_\odot$	ST
Supernova explosion rate of the IS	$\mathcal{R}$	~0.08	SN yr^{-1}	ST
Supernova explosion rate of the SD	–	~0.01	SN yr^{-1}	ST
Typical supernova explosion energy	–	10^{51}	erg	ST
SN energy transferred to cosmic rays	η	~10	%	ST
Convective velocity	V	300–600	km s^{-1}	ST
Dust emissivity index	σ	1.5	–	OM
Dust temperature	$T_{\rm dust}$	50	K	OM
Emission measure	EM	5×10^5	pc cm^{-6}	OM
Ionized gas temperature	T	10^4	K	OM
Magnetic field of the IS	B	300	μG	OM
Slope of primary injection spectrum	p	2.2–2.3	–	A
Maximum energy considered for primaries	–	100	TeV	A
Diffusion coefficient slope	μ	0.5	–	A
Proton to electron primary ratio	$N_{\rm p}/N_{\rm e}$	50	–	A
Diffusive timescale	τ_0	1–10	Myr	A

for the central nucleus or was already found excessive. The target mass of the innermost region differs from ours by a factor of about 6, ours being smaller. The fraction of the supernova explosion converted into cosmic rays (20% for Paglione et al., a factor of 2 larger than ours) also seems excessive as regards the current measurements of SNR at the highest energies. We also considered a surrounding disk with a smaller supernova rate, following the discovery of several SNRs in that region (Ulvestad 2000), especially to test its influence in the total γ-ray output. Finally, the Paglione et al. (1996) study did not produce results above 200 GeV[2].

The *Q*-DIFFUSE set uses different parameterizations for pion cross sections as compared with those used by Marscher & Brown (1978), whose code was the basis of the Paglione et al. study. Our computation of neutral pion decay γ-rays is discussed in the Appendix. In addition, *Q*-DIFFUSE uses the full inverse Compton Klein-Nishina cross section, computes secondaries (e.g., knock-on electrons) without resorting to parameterizations that are valid only for Earth-like cosmic ray (CR) intensities, fixes the photon target for Compton scattering starting from modelling the observations in the FIR, and considers opacities to γ-ray scape.

5. Results

5.1. Summary of model parameters

We begin the discussion of our results by presenting a summary of the parameters we have used for, and obtained from, our modelling. These are given in Table 1. There, the mark OM refers to *Obtained from modelling* and ST or *see text* refers to parameters discussed in more detail in the previous section on phenomenology, where references are also given. These parameter values or range of values are fixed by observations. Finally, the mark A refers to *assumed parameters*, in general within a range. Variations to the values given in Table 1 are discussed below.

5.2. Steady proton and electron population

The numerical solution of the diffusion-loss equation for protons and electrons, each subject to the losses previously described, is shown in Fig. 1. We adopted a diffusive residence timescale of 10 Myr, a convective timescale of 1 Myr, and a density of ~600 cm^{-3}. In the case of electrons, the magnetic field with which synchrotron losses are computed in Fig. 1 is 300 μG. The latter is fixed below, requiring that the steady electron population produces a flux level of radio emission

[2] To further ease the comparison, we here note some typos in the Paglione et al. (1996) paper: The factor $b(E)$ should be elevated to minus one in their Eq. (4), as well as the term $\tau_{\rm c}$ in their Eq. (3). The y-axis of their Fig. 1 is not the emissivity, but the emissivity divided by the density; units need to be modified accordingly , see e.g. Abraham et al. (1966). $E_{\rm p}$ in their Eq. (7) and x-axis of Figs. 2 and 3 is the kinetic energy, but the generic E in Eq. (1) is the total energy. The y-axis of Fig. 2 is in units of cm^{-3} GeV^{-1}.

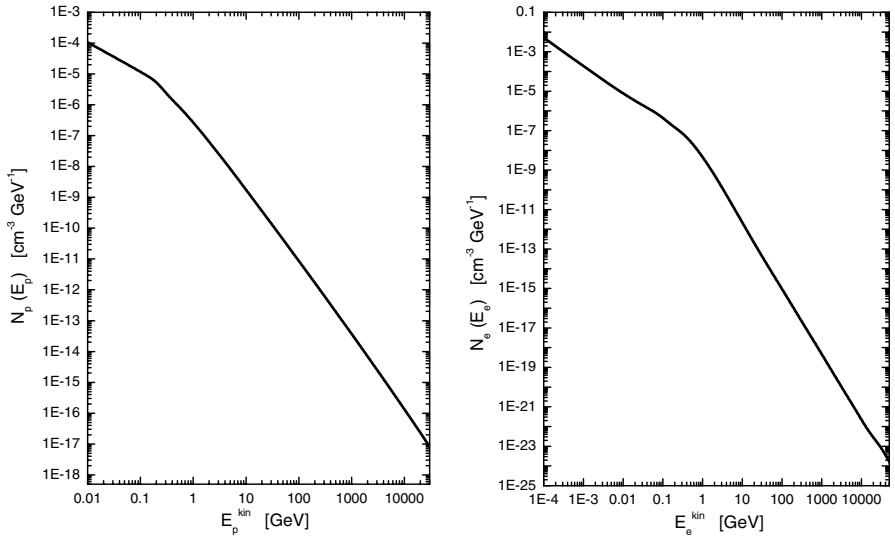

Fig. 1. Steady proton (*left panel*) and electron (*right panel*) distributions in the innermost region of NGC 253.

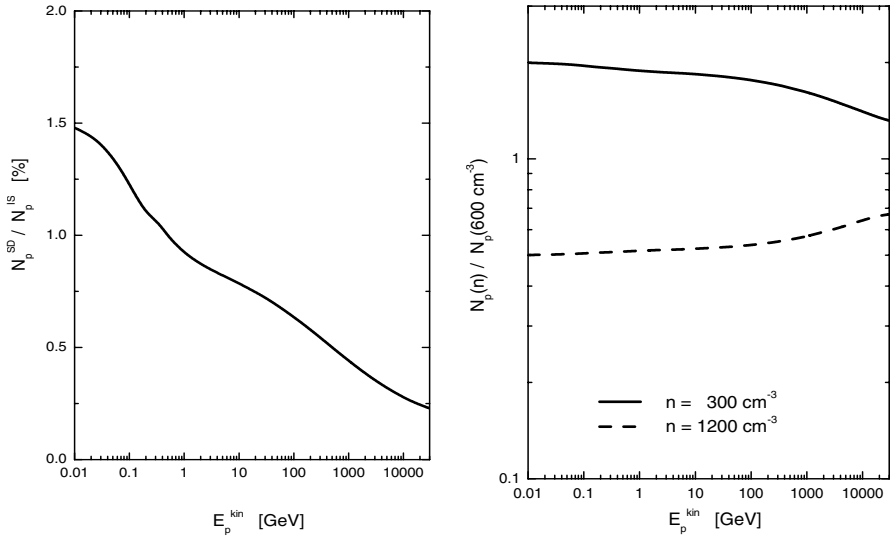

Fig. 2. *Left*: ratio of the steady proton population in the surrounding disk to that in the innermost starburst region. *Right*: ratio between the steady proton distribution in the IS, when the gas density is artificially enhanced and diminished by a factor of 2.

matching observations. An injection electron spectrum is considered – in addition to the secondaries – in generating the steady electron distribution. The primary electron spectrum is assumed as that of the protons times a scaling factor, the inverse of the ratio between the number of protons and electrons, $N_\mathrm{p}/N_\mathrm{e}$ (e.g., Bell 1978). This ratio is about 100 for the Galaxy, but could be smaller in star-forming regions, where there are multiple acceleration sites. For instance, Völk et al. (1989) obtained $N_\mathrm{p}/N_\mathrm{e} \sim 30$ for M 82, where $N_\mathrm{p}/N_\mathrm{e} = 50$ is assumed for the central disk of NGC 253. From about $E_\mathrm{e} - m_\mathrm{e} \sim 10^{-1}$ to ∼10 GeV, the secondary population of electrons (slightly) dominates, in any case. This is shown in Fig. 3. It is in this region of energies where most of the synchrotron radio emission is generated, such that the ability to produce a high energy model compatible with radio observations is a cross check for the primary proton distribution.

Figure 2 shows the ratio of the steady proton population in the SD to that in the IS. Because the SD is subject to a smaller supernova explosion rate, it has a smaller number of protons in its steady distribution, at all energies, on the order of 1% of that of the IS. Then, it will play a subdominant role in the generation of γ-ray emission, as we show below. In the right panel of Fig. 2, and for further discussion in the following sections, we present the ratio between the steady proton distribution in the IS, when the gas density is artificially enhanced and diminished by a factor of 2 from the assumed value of 600 cm^{-3}.

5.3. IR and radio emission

The continuum emission from NGC 253, at wavelengths between ∼1 cm and ∼10 microns, was measured by several authors, e.g., see Fig. 4 and Sect. 3. Due to angular resolution, these observations did not in general distinguish only the emission coming from the innermost starburst region. Instead, they also contain a contribution from the photons produced in the surrounding disk and farther away from the nucleus.

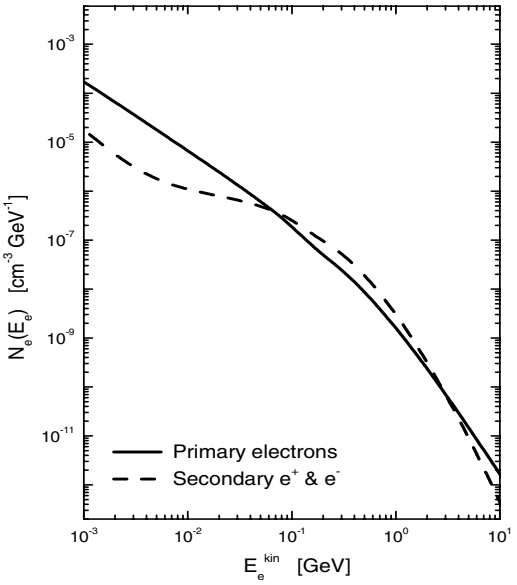

Fig. 3. Steady population of primary-only and secondary-only electrons. Only the region of the secondary dominance of the distribution is shown.

The IR continuum emission is mainly produced thermally by dust, and thus it could be modelled with a spectrum having a dilute blackbody (graybody) emissivity law, proportional to $\nu^{\sigma} B(\epsilon, T)$, where B is the Planck function. Figure 4 shows the result of this modelling and its agreement with observational data when the dust emissivity index $\sigma = 1.5$, and the dust temperature $T_{\rm dust} = 50$ K. Different total luminosities, i.e. the normalization of the dust emission (see the appendix of Torres 2004 for details), are shown in the figure to give an idea of the contribution of the innermost region with respect to that of the rest of the galaxy. According to Melo et al. (2002), about half of the total IR luminosity is produced in the IS, which is consistent with the data points being intermediate between the curves with $L_{\rm IR}$ 2×10^{10} and 4×10^{10} $L_{\odot}$, since the latter were obtained with beamsizes of about 20–50 arcsec (~240–600 pc at the NGC 253 distance).

The influence of the magnetic field upon the steady state electron distribution is twofold. On one hand, the greater the field, the larger the synchrotron losses – which is particularly visible at high energies, where synchrotron losses play a relevant role. On the other, the larger the field, the smaller the steady distribution. These effects evidently compete with each other in determining the final radio flux. The magnetic field is required to be such that the radio emission generated by the steady electron distribution is in agreement with the observational radio data. This is achieved by iterating the feedback between the choice of magnetic field, the determination of the steady distribution, and the computation of radio flux, additionally taking free-free emission and absorption processes into account. While free-free emission is subdominant when compared with the synchrotron flux density, free-free absorption plays a key role at low frequencies, determining the opacity. We have found a reasonable agreement with all observational data for a magnetic field in the innermost region of 300 μG, an ionized gas temperature of about 10^4 K, and an emission measure of 5×10^5 pc cm^{-6}, the latter two in separate agreement with the free-free modelling of the opacity of particular radio sources, as discussed in Sect. 3. The value of magnetic field we found for the IS is very similar to the one found for the disk of Arp 220 (Torres 2004) and compatible with measurements in molecular clouds (Crutcher 1988, 1994, 1999).

5.4. γ-ray emission

In the left panel of Fig. 5, bremsstrahlung, inverse Compton, and pion decay γ-ray fluxes of the IS are shown together with the total contribution of the SD and the total differential flux of the whole system. These results are obtained with the model that was just shown to be in agreement with radio and IR observations. As mentioned before, the contribution of the SD, even when having a factor of ~8 more mass than the IS, is subdominant. The reason for this is that this region is much less active (Ulvestad 2000).

While complying with EGRET upper limits, our predictions are barely below them. If this model is correct, NGC 253 is bound to be a bright γ-ray source for GLAST.

The integral fluxes are shown in the right panel of Fig. 5. Our model again complies with the integral EGRET upper limit for photons above 100 MeV, and predicts that, given enough observation time, NGC 253 will also appear as a point-like source in an instrument like HESS. Note, however, that quite a long exposure may be needed to detect the galaxy and also that our fluxes are only a few percent of those reported by the CANGAROO collaboration.

An additional source of TeV photons not considered here is the hadronic production in the winds of massive stars (Romero & Torres 2003). However, a strong star-forming region, such as the nucleus of NGC 253, is bound to possess much more free gas than that contained within the winds of massive stars, which albeit numerous, have mass loss rates typically in the range of 10^{-6}–10^{-7} $M_{\odot}$[3].

5.5. Opacities to γ-ray escape

Two sources of opacities are considered: pair production from the γ-rays interaction with the photon field or with the charged nucleus present in the medium. Compton scattering and attenuation in the magnetic field by one-photon pair production are negligible.

The opacity to $\gamma\gamma$ pair production with the photon field, which at the same time is the target for inverse Compton processes, can be computed as $\tau(R_{\rm c}, E_{\gamma})^{\gamma\gamma} = \int\int_{R_c}^{\infty} n(\epsilon)\sigma_{\rm e^-e^+}(\epsilon, E_{\gamma})^{\gamma\gamma} {\rm d}r\, {\rm d}\epsilon < \tau(E_{\gamma})^{\gamma\gamma}_{\rm max} < (h/\cos(i)) \times \int_0^{\infty} n(\epsilon)\sigma_{\rm e^-e^+}(\epsilon, E_{\gamma}){\rm d}\epsilon$, where ϵ is the energy of the

[3] In Romero & Torres (2003), higher mass loss rates up to 10^{-5} $M_{\odot}$, i.e., grammages between 50 and 150 g cm^{-2}, were allowed. Although found in perhaps one or two Galactic early O stars, these values are uncommon. Since the size of the base of the wind for each star, the grammage, and the ambient enhancement of cosmic rays were independently allowed to take values within their assumed ranges in the Monte Carlo simulation of Romero & Torres (2003), the stars with the most favorable parameters would dominate the sum, overestimating the relative importance of their fluxes.

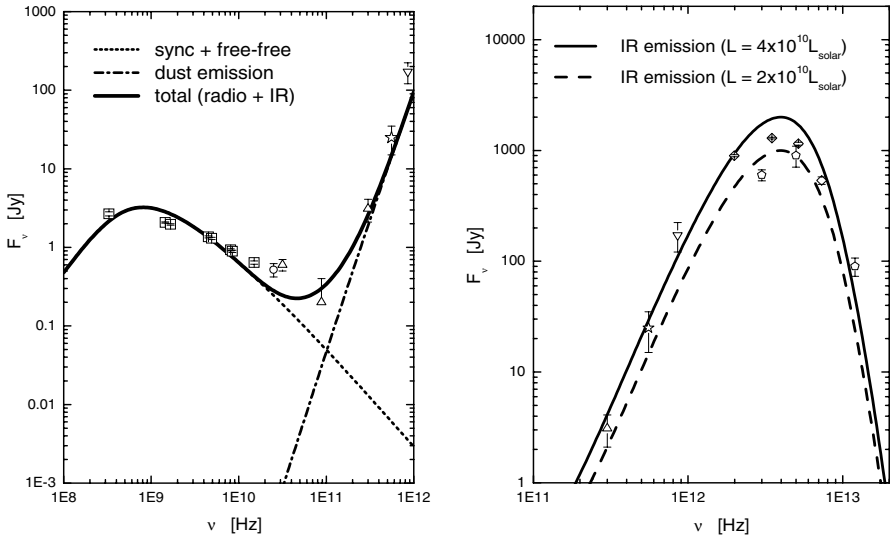

Fig. 4. *Left*: multifrequency spectrum of NGC 253 from radio to IR, with the result of our modelling. The experimental data points correspond to: pentagons, Melo et al. (2002); diamonds, Telesco et al. (1980); down-facing triangles, Rieke et al. (1973); stars, Hildebrand et al. (1977); up-facing triangles, Elias et al. (1978); circles, Ott et al. (2005); squares, Carilli (1996). *Right*: IR flux from NGC 253 assuming a dilute blackbody with temperature $T_{\rm dust} = 50$ K and different total luminosities.

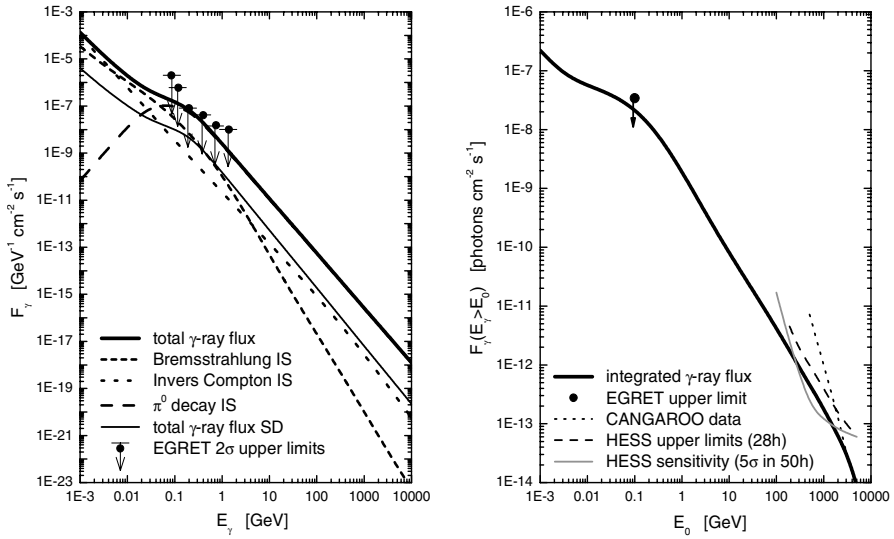

Fig. 5. *Left*: differential γ-ray fluxes from the central region of NGC 253. Total contribution of the surrounding disk is shown separately, as are the EGRET upper limits. In the case of the IS, we show the relative contributions of bremsstrahlung, inverse Compton, and neutral pion decay to the γ-ray flux separately. *Right*: integral γ-ray fluxes. The EGRET upper limit (for energies above 100 MeV), the CANGAROO integral flux as estimated from their fit, and the HESS sensitivity (for a 5σ detection in 50 h) are given. Absorption effects are already taken into account. Also shown is the recently released HESS upper limit curve on NGC 253.

target photons, E_γ is the energy of the γ-ray in consideration, $R_{\rm c}$ is the place where the γ-ray photon was created within the system, and $\sigma_{\rm e^-e^+}(\epsilon, E_\gamma)^{\gamma\gamma} = (3\sigma_{\rm T}/16)(1-\beta^2)(2\beta(\beta^2-2)+(3-\beta^4)\ln((1+\beta)/(1-\beta)))$, with $\beta = (1-(mc^2)^2/(\epsilon E_\gamma))^{1/2}$ and $\sigma_{\rm T}$ being the Thomson cross section, is the cross section for $\gamma\gamma$ pair production (e.g. Cox 1999, p. 214). Note that the lower limit of the integral on ϵ in the expression for the opacity is determined from the condition that the center of mass energy of the two colliding photons should be such that $\beta > 0$. The fact that the dust within the starburst reprocesses the UV star radiation to the less energetic infrared photons implies that the opacities to $\gamma\gamma$ process is significant only at the highest energies. No source of this kind of opacity is assumed outside the system under consideration, since the nearness of NGC 253 makes the opacity generated by cosmological fields negligible.

The cross section for pair production from the interaction of a γ-ray photon in the presence of a nucleus of charge Z in the completely screened regime ($E_\gamma/mc^2 \gg 1/(\alpha Z)$) is independent of energy and is given by (e.g. Cox 1999, p. 213) $\sigma^{\gamma Z}_{\rm e^-e^+} = (3\alpha Z^2\sigma_{\rm T}/2\pi)(7/9\ln(183/Z^{1/3}) - 1/54)$. At lower energies, the relevant cross section is that of the no-screening

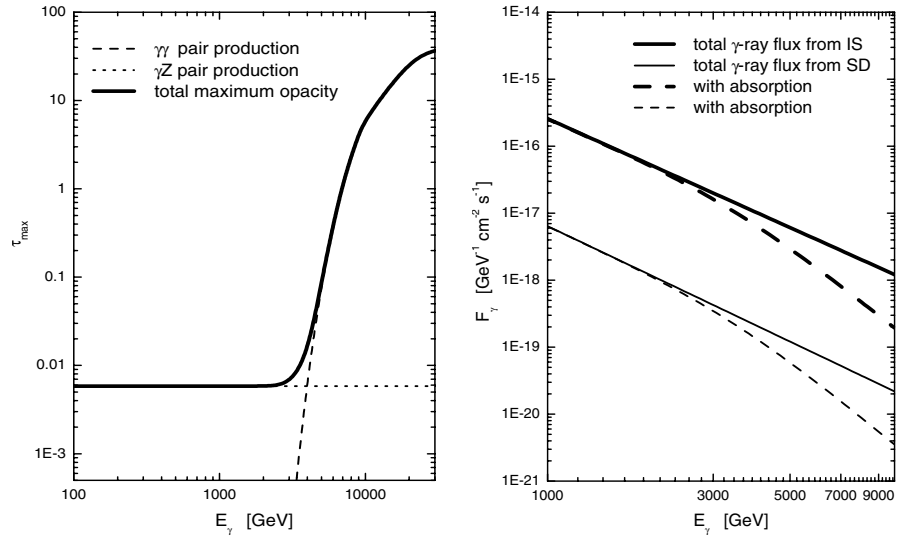

Fig. 6. *Left*: opacities to γ-ray scape as a function of energy. The highest energy is dominated by $\gamma\gamma$ processes, whereas γZ dominates the opacity at low energies. Significant $\tau_{\rm max}$ are only encountered above 1 TeV. *Right*: modification of the γ-ray spectrum introduced by the opacity to γ-ray escape.

Table 2. Exploring the parameter space for p and τ_0. The results of our adopted model are given in the first column. These results already take the opacity to photon escape into account.

$F(E > E_0)$	$p = 2.3$ $\tau_0 = 10$ Myr	$p = 2.3$ $\tau_0 = 5$ Myr	$p = 2.3$ $\tau_0 = 1$ Myr	$p = 2.2$ $\tau_0 = 10$ Myr	$p = 2.2$ $\tau_0 = 5$ Myr	$p = 2.2$ $\tau_0 = 1$ Myr
$E_0 = 100$ MeV	2.32E-8	2.36E-8	2.21E-8	2.95E-8	2.97E-8	2.75E-8
$E_0 = 200$ GeV	1.60E-12	1.23E-12	4.76E-13	4.04E-12	3.08E-12	1.15E-12
$E_0 = 600$ GeV	3.61E-13	2.67E-13	8.98E-14	1.00E-12	7.34E-13	2.40E-13
$E_0 = 1$ TeV	1.78E-13	1.29E-13	4.10E-14	5.16E-13	3.70E-13	1.14E-13
$E_0 = 2$ TeV	6.29E-14	4.46E-14	1.31E-14	1.92E-13	1.35E-13	3.87E-14

case, which has a logarithmic dependency on energy, $\sigma^{\gamma Z}_{e^-e^+} = (3\alpha Z^2\sigma_{\rm T}/2\pi)(7/9\ln(2E_\gamma/mc^2) - 109/54)$, and matches the complete screening cross section at around 0.5 GeV. Both of these expressions are used to compute the opacity, depending on E_γ.

In the left panel of Fig. 6 we show the different contributions to the opacity. The equation of radiation transport appropriate for a disk is used to compute the predicted γ-ray flux taking all absorption processes into account (see appendix in Torres 2004 for details). The right panel of Fig. 6 shows the effect of the opacity on the integral γ-ray fluxes, only evident above 3 TeV.

5.6. Exploring the parameter space and degeneracies

As summarized in Table 1, most of the model parameters are well fixed from observations. There are, however, a couple of assumptions which may produce slight degeneracies, while not being well bounded from experiments. Consider for instance the proton injection slope p and the diffusive scale τ_0. For the former we have assumed $p = 2.3$, which agrees with the recent results from HESS regarding γ-ray observations at TeV energies of supernova remnants and unidentified extended sources. However, it would certainly be within what one would expect from proton acceleration in supernova remnants, and also within experimental uncertainty, if a better description for the average proton injection slope in NGC 253 is 2.2 instead of 2.3. Table 2 shows the influence of this kind of choice on our final results. A harder slope slightly increases the integral flux. Similarly, the diffusive timescale is not well-determined, and it may be arguable perhaps within one order of magnitude. Table 2 also shows the influence of this choice. Ultimately, high energy γ-ray observations (from GeV to TeV) are the ones to impose constraints on these values. In any case, we notice that pp interaction and convection timescales are much shorter (<1 Myr), thus dominating the form of $N(E)$. To show this in greater detail, we give the result for the proton distribution in Fig. 7 when different convective and the pp timescales are taken into account as compared with the solution when $\tau(E) = \tau_{\rm D}$, i.e., diffusion only. Clearly, convection plus pp timescales dominates the spectrum.

Regarding degeneracies, both the proton slope and the confinement timescales, however, cannot be much different from what we have assumed. If the former were to differ significantly, it would be impossible to reproduce the radio data, which is the result of the synchrotron emission of the secondary electrons. Changes in the number of protons in the IS would imply a change in the magnetic field to reproduce radio observations, which clearly cannot be pushed much either.

In a less impacting way, varying the value of $N_{\rm p}/N_{\rm e}$ can also vary the results. This variation would be slight because of the

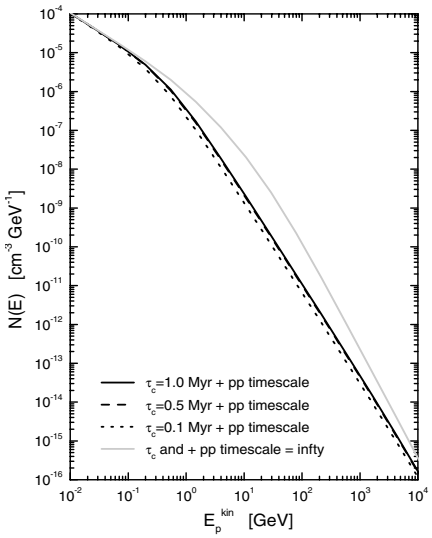

Fig. 7. Proton distribution when different convective and the pp timescales are taken into account as compared with a (arbitrary) solution when $\tau(E) = \tau_D$, i.e., diffusion only. Clearly, convection plus pp timescales dominates the spectrum.

Table 3. The effect of the medium gas density on the γ-ray integral fluxes. Results provided are in units of photons cm^{-2} s^{-1}, and already take the opacity to photon escape into account.

$F(E > E_0)$	n = 300 cm^{-3}	n = 600 cm^{-3}	n = 1200 cm^{-3}
E_0 = 100 Mev	2.22E-8	2.32E-8	2.37E-8
E_0 = 200 Gev	1.20E-12	1.60E-12	1.95E-12
E_0 = 600 Gev	2.60E-13	3.61E-13	4.52E-13
E_0 = 1 Tev	1.26E-13	1.78E-13	2.26E-13
E_0 = 2 Tev	4.36E-14	6.29E-14	8.09E-14

influence of the more numerous secondary electrons in the energetic region of interest for radio emission. On the same track, varying the diffusion coefficient μ does not cause substantial changes. Finally, if the maximum proton energy were to differ from the value of 100 TeV we have assumed, the end of the spectrum would accordingly shift slightly, but we do not expect it to happen in a significant way, since we do now observationally know that supernova remnants are sources of ∼10 TeV photons.

Even within an artificially enlarged uncertainty of the gas density, the results will not be modified much; if for any reason the average particle density were to be a factor of 2 smaller or larger, the γ-ray integral flux variations would be within 4% for energies above 100 MeV, and within 25% for energies above 200 GeV. Table 3 shows these results by presenting the integral fluxes above a given threshold if the assumed density of 600 cm^{-3} is doubled or halved. As can be seen in the right panel of Fig. 2, if the density is larger (smaller) by a factor ∼2, the resulting steady proton distribution from the same proton injection population is smaller (bigger) by a similar factor over a wide range of proton energies. As γ-ray emissivities are proportional to both the medium density and the number of steady protons, the variations in γ-ray fluxes are compensated for quite well.

5.7. Energetics and cosmic ray enhancement

The left panel of Fig. 8 presents the energy density contained in the steady proton population above a certain energy; i.e., based on Fig. 1, the curve shows the integral $\int_E N_{\rm p}(E_{\rm p})\, E_{\rm p}\, {\rm d}E_{\rm p}$. The total energy density contained by the steady population of cosmic rays above 1 GeV is about 10^{-3} of the power emitted by all supernova explosions in the last 5 million years. The energy density contained in the steady electron population is several orders of magnitude less important.

The cosmic ray enhancement is a useful parameter in estimating γ-ray luminosities in different scenarios. It is defined as the increase in the cosmic ray energy density with respect to the local value, $\omega_{\rm CR,\odot}(E) = \int_E N_{\rm p\oplus}(E_{\rm p}) E_{\rm p} {\rm d}E_{\rm p}$, where $N_{\rm p\oplus}$ is the local cosmic ray distribution obtained from the measured cosmic ray flux that we quote in the Appendix. The enhancement factor ς is then a function of energy given by $\varsigma(E) = (\int_E N_{\rm p}(E_{\rm p})\, E_{\rm p}\, {\rm d}E_{\rm p})/\omega_{\rm CR,\odot}(E)$. Values of enhancement for NGC 253 were proposed $\varsigma \leq 3000$ for energies above 1 GeV (e.g., Suchkov et al. 1993), and we can actually verify this in our model. The right panel of Fig. 8 presents the enhancement factor as a function of proton energy. The larger the energy, the larger the enhancement, due to the steep decline ($\propto E^{-2.75}$) of the local cosmic ray spectrum.

6. HESS observations

The HESS array has just released (Aharonian et al. 2005c) their results for NGC 253. These are based on data taken during the construction of the array with 2 and 3 telescopes operating. The total observation time was 28 hs, with a mean zenith angle of about 14 degrees. Only events where at least two telescopes were triggered were used, to enable stereoscopic reconstruction. The energy threshold for this dataset was 190 GeV. Upper limits from HESS on the integral flux of γ-rays from NGC 253 (99% confidence level) are shown, together with our predictions, in the right panel of Fig. 5, and zoomed in the region above 100 GeV in Fig. 9. As an example, above 300 GeV, the upper limit is 1.9×10^{-12} photons cm^{-2} s^{-1}. It can be seen that our predictions are below these upper limits at all energies but still above HESS sensitivity for reasonable observation times.

7. Concluding remarks

We have presented a multifrequency model of the central region of NGC 253. Following recent observations, we modelled an innermost starburst with a radius of 100 pc and a supernova explosion rate of 0.08 yr^{-1}, and with a surrounding disk up to a 1 kpc in radius with an explosion rate about tenfold smaller. As a result of our modelling, we found that a magnetic field of 300 μG for the innermost region is consistent with high resolution radio observations, with the radiation at 1 GHz mostly produced by secondary electrons of cosmic ray interactions. The magnetic field found for the innermost part of NGC 253 is typical of dense molecular clouds in our Galaxy, and is close to the (270 μG) value proposed by Weaver et al. (2002) using the equipartition argument. We estimated free-free emission and absorption, and considered opacities to the γ-ray

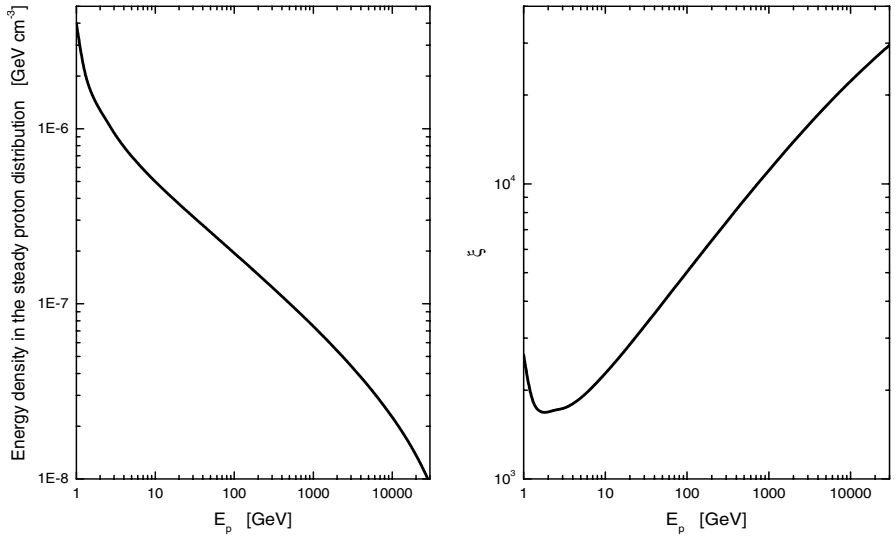

Fig. 8. *Left*: energy density contained in the steady population of protons above the energy given by the *x*-axis. *Right*: cosmic ray enhancement factor obtained from the steady spectrum distribution in the innermost starburst nucleus of NGC 253.

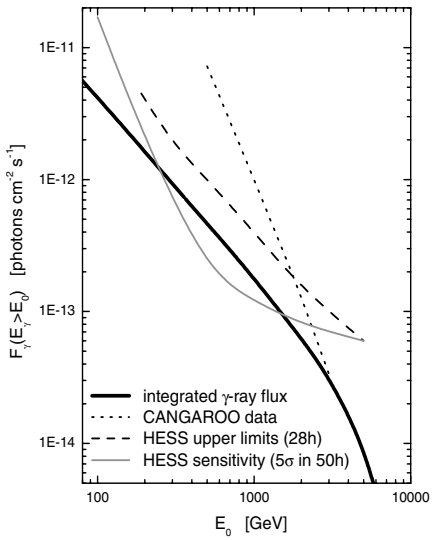

Fig. 9. Integral γ-ray fluxes zoomed in the region above 100 GeV, together with the (2 telescopes) HESS upper limits and the (4 telescopes) HESS sensitivity.

escape. The hard X-ray emission from IC and bremsstrahlung processes produced in this model is below observational constraints, e.g., by OSSE in agreement with previous estimations of bremsstrahlung diffuse emission (Bhattacharya et al. 1994). This is consistent with measurements in the center of the Galaxy, where INTEGRAL have shown that hard X-ray emission is not diffusive, but produced by point-like sources (Lebrun et al. 2004).

The predicted flux is based on a set of a few well-founded assumptions, mainly a) that supernova remnants accelerate most of the cosmic rays in the central region of NGC 253, and b) that they interact with the present gas, whose amount has been measured using a variety of techniques. The low opacity to γ-ray escape ensures that basically all γ-rays produced in the direction towards Earth reach us. Observational constraints establish the values of the supernova explosion rate and gas content (see Sect. 2 for references).

The ease of all the assumptions made in our model, its concurrence with all observational constraints, and the unavoidability of the processes analyzed, all lead us to conclude that: 1) GLAST will detect NGC 253, with our predicted luminosity (2.3×10^{-8} photons cm^{-2} s^{-1} above 100 MeV) well above its 1 yr all-sky survey sensitivity (GLAST Science Requirements Doc. 2003); 2) that our predicted TeV fluxes are about one order of magnitude smaller than what was claimed by CANGAROO and, thus, that perhaps in this case, a similar problem to that found in other sources affected their data taking or analysis, and 3) that HESS could detect the galaxy as a point-like source, provided it is observed long enough with the full array ($\gtrsim$50 h, for a detection between 300 and 1000 GeV)[4]. We finally note that this model predicts a steady γ-ray source, so that a posteriori variability estimators (e.g., Torres et al. 2001) can be checked for consistency.

Acknowledgements. The work of ED-S was done under a FPI grant of the Ministry of Science and Tecnology of Spain. The work of DFT was performed under the auspices of the U.S. D.O.E. (NNSA), by the University of California Lawrence Livermore National Laboratory under contract No. W-7405-Eng-48. We thank Juan Cortina, Igor Moskalenko, and Olaf Reimer for comments. We thank the referee, V. Dogiel, for remarks that led to improvement of this work.

[4] HESS site latitude provides that NGC 253 can be observed very close to the zenith (the minimum zenith angle for NGC 253 from HESS site is 2 degrees). As a consequence, HESS observations of NGC 253 can be performed with the minimum energy threshold of the experiment. The MAGIC Telescope, although at a northern hemisphere site, is also able to observe NGC 253 at a larger zenith angle, about 53 degrees.

References

Abraham, P. B., Brunstein, K. A., & Cline, T. L. 1966, Phys. Rev., 150, 150

Aharonian, F. A., & Atoyan, A. M. 2000, A&A, 362, 937

Aharonian, F. A., Akhperjanian, A. G., Aye, K.-M., et al. 2004a, Nature, 432, 75

Aharonian, F. A., Akhperjanian, A. G., Aye, K.-M., et al. 2004b, A&A, 425, L13

Aharonian, F. A., Akhperjanian, A. G., Aye, K.-M., et al. 2005a, A&A, 437, 135

Aharonian, F. A., Akhperjanian, A. G., Aye, K.-M., et al. 2005b, A&A, 432, L9

Aharonian, F. A., et al. 2005c, A&A, in press

Anchordoqui, L. A., Romero, G. E., & Combi, J. A. 1999, Phys. Rev., D60, 103001

Anchordoqui, L. A., Goldberg, H., & Torres, D. F. 2003, Phys. Rev., D67, 123006

Bhattacharya, D., The, L.-S., Kurfess, J. D., et al. 1994, ApJ, 437, 173

Bell, A. R. 1978, MNRAS, 182, 443

Berezinskii, V. S., Bulanov, S., Dogiel, V., & Ginzburg, V. 1990, Astrophysics of Cosmic Rays, North-Holland

Blattnig, S. R., et al. 2000, Phys. Rev., D62, 094030

Blattnig, S. R., et al. 2000b, NASA/TP-2000-210640, Langley Research Center, available online at http://techreports.larc.nasa.gov/ltrs/PDF/2000/tp/ NASA2000tp210640.pdf

Blom, J. J., Paglione, T. A., & Carramiñana, A. 1999, 516, 744

Bradford, C. M., Nikola, T., Stacey, G. J., et al. 2003, ApJ, 586, 891

Bryant, P. M., & Scoville, N. Z. 1999, ApJ, 117, 2632

Canzian, B., Mundy, L. G., & Scoville, N. Z. 1988, ApJ, 333, 157

Carilli, C. L. 1996, 305, 402

Chevalier, R. A. 1982, ApJ, 289, 302

Crutcher, R. M. 1988, in Molecular Clouds, Milky-Way & External Galaxies, ed. R. Dickman, R. Snell, & J. Young (New York: Springer), 105

Crutcher, R. M. 1994, Clouds, cores and low mass stars, Proceedings of the 4th Haystack Observatory, ed. D. P. Clemens, & R. Barvainis, ASP Conf. Ser., 65, 87

Crutcher, R. M. 1999, ApJ, 520, 706

Cox, A. N. 1999, Allen's Astrophysical Quantities (New York: Springer Verlag)

Cox, P., & Metzger, P. G. 1989, A&ARv, 1, 49

Dermer, C. D. 1986a, A&A, 157, 223

Dermer, C. D. 1986b, ApJ, 307, 47

Downes, D., & Solomon, P. M. 1998, ApJ, 507, 615

Dudley, C. C., & Wynn-Williams, C. G. 1999, MNRAS, 304, 549

Duric, N., Gordon, S. M., Goss, W. M., Viallefond, F., & Lacey, C. 1995, ApJ, 445, 173

Elias, J. H., Neugebauer, G., Werner, M. W., et al. 1978, ApJ, 220, 25

Engelbracht C. W., Rieke M. J., Rieke G. H., Kelly, D. M., & Achterman, J. M. 1998, ApJ, 505, 639

Forbes, D. A., Ward, M. J., Rotaciuc, V., et al. 1993, ApJ, 406, L11

Forbes, D. A., Polehampton, E., Stevens, I. R., Brodie, J. P., & Ward, M. J. 2000, MNRAS, 312, 689

Ginzburg, V. L., & Syrovatskii, S. I. 1964, The origin of cosmic rays (Oxford, England: Pergamon Press)

GLAST Science Requirements Document, 433-SRD-0001, NASA Goddard Space Flight Center, CH-03, 2003, http://glast.gsfc.nasa.gov/project/cm/mcdl

Hagiwara, K., et al. 2002, Phys. Rev., D66, 010001. Data on the total and elastic cross sections are available at http://pdg.lbl.gov/2002/contents_plots.html

Harris, A. I., Stutzki, J., Graf, U. U., Russell, A. P. G., Genzel, R., & Hills, R. E. 1991, ApJ, 382, L75

Harrison, A., Henkel, C., & Russel, A. 1999, MNRAS, 303, 157

Heckman, T. M., Armus, L., & Miley, G. K. 1990, ApJS, 74, 833

Hildebrand, R. H., Whitcomb, S. E., Winston, R., et al. 1977, ApJ, 216, 698

Houghton, S., Whiteoak, J. B., Koribalski, B., et al. 1997, A&A, 325, 923

Hunter, S. D., Bertsch, D. L., Catelli, J. R., et al. 1997, ApJ, 481, 205

Itoh, C., Enomoto, R., Yanagita, S., et al. 2002, A&A, 396, L1

Itoh, C., Enomoto, R., Yanagita, S., et al. 2003, A&A, 402, 443

Israel, F. P., & Baas, F. 2002, A&A, 383, 82

Kamae, T., Abe, T., & Koi, T. 2005, ApJ, 620, 244

Keto, E., Hora, J. L., Fazio, G. G., Hoffman, W., & Deutsch, L. 1999, ApJ, 518, 133

Lebrun, F., Terrier, R., Bazzano, A., et al. 2004, Nature, 428, 293

Longair M. S. 1994, High Energy Astrophysics, Vol.2: Stars, the Galaxy and the Interstellar Medium (Cambridge University Press), 2nd ed.

Mannheim, K., & Schlickeiser, R. 1994, A&A, 286, 983

Marscher, A. P., & Brown, R. L. 1978, ApJ, 221, 588

Mauersberger, R., Henkel, C., Wiebelinski, R., Wiklind, T., & Reuter, H.-P. 1996, A&A, 305, 421

McCarthy, P. J., Heckman, T., & van Breugel, W. 1987, AJ, 92, 264

Mao, R. Q., Henkel, C., Schulz, A., et al. 2000, A&A, 358, 433

Melo, V. P., Perez-Garcia, A. M., Acosta-Pulido, J. A., Muñoz-Tuñon, & Rodriguez Espinosa, J. M. 2002, ApJ, 574, 709

Moskalenko, I., & Strong, A. W. 1998, ApJ, 493, 694

Ott, J., Weiss, A., Henkel, C., & Walter, F. 2005 [arXiv:astro-ph/0505143], In Starbursts: From 30 Doradus to Lyman Break Galaxies, Held in Cambridge, UK, 6–10 September 2004, ed. R. de Grijs, & R. M. Gonzalez Delgado, Astrophysics & Space Science Library (Dordrecht: Springer), 329, P57

Paglione, T. A. D., Tosaki, T., & Jackson, J. M. 1995, ApJ, 454, L117

Paglione, T. A. D., Marscher, A. P., Jackson, J. M., & Bertsch, D. L. 1996, ApJ, 460, 295

Paglione, T. A. D., Jackson, J. M., & Ishizuki, S. 1997, ApJ, 484, 656

Paglione, T. A. D., Yam, O., Tosaki, T., & Jackson, J. M. 2004, ApJ, 611, 835

Pavlidou, V., & Fields, B. 2001, ApJ, 558, 63

Pence, W. D. 1981, ApJ, 247, 473

Pietsch, W., Roberts, T. P., Sako, M., et al. 2001, A&A, 365, L174

Rice, G. H., et al. 1988, ApJ, 238, 24

Rieke, G. H., Harper, D. A., Low, F. J., & Armstrong, K. R. 1973, ApJ, 83, L67

Rieke, G. H., Lebofsky, M. J., Thompson, R. I., Low, F. J., & Tokunga, A. T. 1980, ApJ, 238, 24

Rieke, G. H., Lebofsky, M. J., & Walker, C. E. 1988, ApJ, 325, 679

Romero G. E., & Torres, D. F. 2003, ApJ, 586, L33

Suchkov, A., Allen, R. J., & Heckman, T. M. 1993, ApJ, 413, 542

Solomon, P. M., Downes, D., Radford, S. J. E., & Barrett, J. W. 1997, ApJ, 478, 144

Sorai, K., Nakai, N., Nishiyama, K., & Hasegawa, T. 2000, Publ. Astron. Soc. Japan, 52, 785

Sreekumar, P., Bertsch, D. L., Dingus, B. L., et al. 1992, ApJ, 400, L67

Stecker, F. W. 1971, Cosmic Gamma Rays (Baltimore: Mono)

Stephens, S. A., & Badhwar, G. D. 1981, Ap&SS, 76, 213

Strickland, D. K., Heckman, T. M., Weaver, K. A., & Dahlem, M. 2000, AJ, 120, 2965

Strickland, D. K., Heckman, T. M., Weaver, K. A., et al. 2002, ApJ, 568, 689

Strong, A. W., Moskalenko, I. V., & Reimer, O. 2000, ApJ, 537, 763

Sugai, H., Davies, R. I., & Ward, M. J. 2003, ApJ, 584, L9
Telesco, C. M., & Harper, D. A. 1980, ApJ, 235, 392
Tingay, S. J. 2004, ApJ, 127, 10
Torres, D. F. 2004a, ApJ, 617, 966
Torres, D. F. 2004b, Published in Gamma-ray Sources, ed. K. S. Cheng, & G. E. Romero (The Netherlands: Kluwer Academic Press), 69 [arXiv:astro-ph/0308069]
Torres, D. F., Romero, G. E., Combi, J. A., et al. 2001, A&A, 370, 468
Torres, D. F., Romero, G. E., Dame, T. M., Combi, J. A., & Butt, Y. M. 2003, Phys. Rep., 382, 303
Torres, D. F., Reimer, O., Domingo-Santamaría, E., & Digel, S. 2004, ApJ, 607, L99
Torres, D. F., & Anchordoqui, L. A. 2004, Rep. Progr. Phys., 67, 1663
Turner, J. L., & Ho, P. T. P. 1985, ApJ, 299, L77
Ulvestad, J. S. 2000, ApJ, 120, 278
Ulvestad, J. S., & Antonucci, R. R. J. 1997, ApJ, 488, 621
Van Buren, D., & Greenhouse, M. 1994, ApJ, 431, 640
Völk, H. J., Klien, U., & Wielebinski, R. 1989, A&A, 237, 21
Völk, H., Aharonian, F. A., & Breitschwerdt, D. 1996, Space Sci. Rev., 75, 279
Ward, J. S., Zmuidzinas, J., Harris, A., & Isaac, K. 2003, ApJ, 587, 171
Weaver, K. A., Heckman, T. M., Strickland, D. K., & Dahlem, M. 2002, ApJ, 576, L19
Wild, W., Bertsch, D. L., Dingus, B. L., et al. 1992, A&A, 265, 447
Watson, A. M., et al. 1996, AJ, 112, 534
Whitmore, J. 1974, Phys. Rept. 10C, 273

Online Material

Appendix: Parameterizations of proton–proton cross sections for neutral pion decay

The π^0 emissivity resulting from an isotropic intensity of protons, $J_{\rm p}(E_{\rm p})$, interacting with fixed target nuclei with number density n, through the reaction $\mathrm{p+p} \rightarrow \mathrm{p+p+}\pi^0 \rightarrow \mathrm{p+p+}2\gamma$, is given by (e.g., Stecker 1971)

$$Q_{\pi^0}(E_{\pi^0}) = 4\pi n \int_{E_{\rm th}(E_{\pi^0})}^{E_{\rm p}^{\rm max}} {\rm d}E_{\rm p}\, J_{\rm p}(E_{\rm p}) \frac{{\rm d}\sigma(E_{\pi^0}, E_{\rm p})}{{\rm d}E_{\pi^0}}, \quad (4)$$

where $E_{\rm p}^{\rm max}$ is the maximum energy of protons in the system, and $E_{\rm th}(E_{\pi^0})$ is the minimum proton energy required to produce a pion with total energy E_{π^0}. The integral lower limit is determined through kinematical considerations. It is basically obtained using the invariant, $\sqrt{s} = \left(2m_{\rm p}(E_{\rm p} + m_{\rm p})\right)^{1/2} = (M_X^2 + E_\pi^{*2} - m_\pi^2)^{1/2} + E_\pi^{*2}$, where s is the square of the total energy in the center-of-mass system, M_X depends on the reaction channel and represents the invariant mass of the system consisting of all particles except the pion, and E_π^* is the CMS energy of the produced meson, which is connected with the laboratory system energy via a Lorentz transformation (see appendices of Moskalenko & Strong 1998 and Blattnig et al. 2000b). Then, $E_\pi^* = (s - M_x^2 + m_\pi^2)/(2\sqrt{s})$, so that for a given value of s, E_π^* will be maximum when M_x takes its minimum value. For the case of neutral pion production, $M_x = 2\,m_{\rm p}$. The laboratory system pion energy, obtained from E_π^*, can be put as a function of s. Inverting this relation, thus obtaining $s = s(E_\pi)$, and using $s = s(E_\pi) = 2m_{\rm p}(E_{\rm p} + m_{\rm p})$ allow for the minimum proton energy to be derived. Finally, ${\rm d}\sigma(E_{\pi^0}, E_{\rm p})/{\rm d}E_{\pi^0}$ is the differential cross section for the production of a pion with energy E_{π^0} in the lab frame, due to a collision of a proton of energy $E_{\rm p}$ with a hydrogen atom at rest.

The γ-ray emissivity is obtained from the neutral pion emissivity Q_{π^0} as

$$Q_\gamma(E_\gamma)_\pi = 2 \int_{E_{\pi^0}^{\rm min}(E_\gamma)}^{E_{\pi^0}^{\rm max}(E_{\rm p}^{\rm max})} {\rm d}E_{\pi^0} \frac{Q_{\pi^0}(E_{\pi^0})}{(E_{\pi^0}^2 - m_{\pi^0}^2 c^4)^{1/2}} \quad (5)$$

where $E_{\pi^0}^{\rm min}(E_\gamma) = E_\gamma + m_{\pi^0}^2 c^4/(4E_\gamma)$ is the minimum pion energy required to produce a photon of energy E_γ (e.g., Stecker 1971), and $E_{\pi^0}^{\rm max}(E_{\rm p}^{\rm max})$ is the maximum pion energy that the population of protons can produce. It is obtained using the invariant equation for the maximum proton energy resident in the system.

As a result, an accurate knowledge of the differential cross section for pion production becomes very important to estimate the γ-ray emissivity. Note that ${\rm d}\sigma(E_{\pi^0}, E_{\rm p})/{\rm d}E_{\pi^0}$ can be thought to contain the inclusive total inelastic cross section (i.e. the cross section multiplied by the average pion multiplicity). This can be stated explicitly as, for instance, in Dermer's (1986a) Eq. (3).

δ-function approximation

In this formalism (Aharonian & Atoyan 2000),

$$\begin{aligned} Q_{\pi^0}(E_{\pi^0}) &= 4\pi n \int_{E_{th}(E_{\pi^0})} {\rm d}E_{\rm p}\, J_{\rm p}(E_{\rm p})\, \delta(E_{\pi^0} - \kappa E_{\rm kin})\, \sigma(E_{\rm p}), \\ &= \frac{4\pi n}{\kappa} J_{\rm p}\left(m_{\rm p}c^2 + \frac{E_{\pi^0}}{\kappa}\right) \sigma\left(m_{\rm p}c^2 + \frac{E_{\pi^0}}{\kappa}\right) \end{aligned} \quad (6)$$

where σ is the total cross-section of inelastic pp collisions, and κ is the mean fraction of the kinetic energy $E_{\rm kin} = E_{\rm p} - m_{\rm p}c^2$ of the proton transferred to the secondary meson per collision. In a broad region from GeV to TeV energies, $\kappa \sim 0.17$. In this approximation, then, an accurate knowledge of the total inelastic cross section is needed to compute the γ-ray emissivity.

Aharonian & Atoyan (2000) propose that, since the cross section appears to rise rapidly from the threshold at $E_{\rm kin} \sim 0.3$ GeV to about 30 mb at energies about $E_{\rm kin} \sim 2$ GeV, and since after that energy it increases only logarithmically, a sufficiently good approximation is to assume

$$\begin{aligned} &\sigma \sim 30\,(0.95 + 0.06\ln(E_{\rm kin}/{\rm GeV}))\,{\rm mb} \quad \text{for} \quad E \geqslant 1{\rm GeV}, \\ &\sigma \sim 0 \quad \text{for} \quad E < 1\ {\rm GeV}. \end{aligned} \quad (7)$$

It can be seen (e.g., Dermer 1986a) that different parameterizations of the cross section below 1 GeV do not noticeably affect the results of γ-ray emissitivities, since most of the γ-rays are generated by primary protons having more energy than a few GeV, provided the spectrum of primaries is sufficiently broad.

In a recent paper, Kamae et al. (2005) introduced the effect of diffractive interactions and scaling violations in $\mathrm{pp} \rightarrow \pi^0$ interactions. The diffractive interactions' contribution was usually neglected in all the other computations of γ-ray emissivity from neutral pion decay to date, and thus one would expect an increase in the predicted fluxes. The best model by Kamae et al., dubbed A, for the inelastic (not inclusive) cross section is given in Table 1 of their paper, Cols. 2 and 3. When one compares the sum of both diffractive and non-diffractive contributions of the Kamae et al. model with Aharonian and Atoyan's formula, one sees that the latter produces an actually larger (but quite close) cross section. Figure 10 shows these results above proton kinetic energies of 1 GeV, as well as the difference between these cross sections. Kamae et al.'s model A was compared with Hagiwara's (2002) compilation of pp cross section measurements and found to be in good agreement. When multiplicity is taken into account, Kamae et al.'s model also agrees with the data on inclusive cross sections, a point we discuss in more detail below.

Figure 11 shows a comparison of the γ-ray emissivity obtained when using Kamae et al.'s model A and Eq. (6). Curves are practically indistinguishable in this scale, and their ratio is well within a factor of ∼1.3. In this comparison, the proton spectrum is the Earth-like one, $J_{\rm p}(E_{\rm p}) = 2.2\,E_{\rm p}^{-2.75}$ protons cm^{-2} s^{-1} sr^{-1} GeV^{-1} and $n = 1$ cm^{-3}. The resulting γ-ray emissivity is multiplied by 1.45 to account for the contribution to the pion spectrum produced in interactions with heavier nuclei both as targets and as projectiles (Dermer 1986a). Aharonian and Atoyan's expression for the cross section pro-

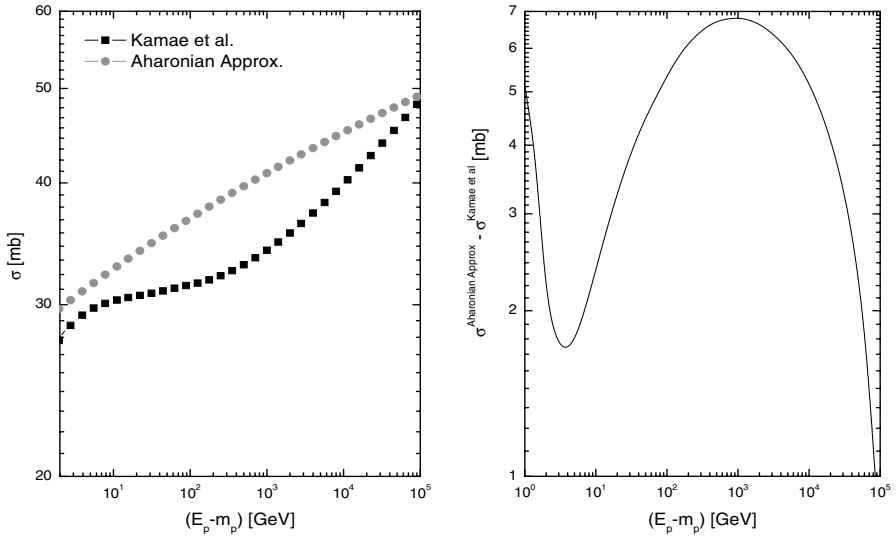

Fig. 10. Comparing sum of diffractive and non-diffractive contributions Kamae et al. model A with Aharonian and Atoyan's formula for the total inelastic cross section.

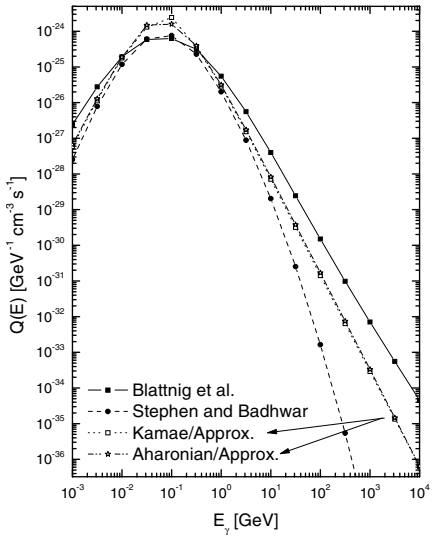

Fig. 11. Comparing γ-ray emissivities within the δ-function approximation (Kamae et al.'s model A and Aharonian and Atoyan's formula for the inelastic cross section) with computations using differential cross section parameterizations.

duces a slightly larger value of emissivity than that obtained with Kamae's model A, including non-diffractive interactions.

Differential cross section parameterizations

Recently, Blattnig et al. (2000) developed parameterizations of the differential cross sections. They have presented a parameterization of the Stephens & Badhwar's (1981) model by numerically integrating the Lorentz-invariant differential cross section (LIDCS). The expression of such parameterization is divided into two regions, depending on the (laboratory frame) proton energy (Blattnig et al. 2000, see their Eqs. (23) and (24)). Blattnig et al. have also developed an alternative parameterization that has a much simpler analytical form. It is given by

$$\frac{\mathrm{d}\sigma(E_{\pi^0}, E_\mathrm{p})}{\mathrm{d}E_{\pi^0}} = e^A \,\mathrm{mb\ GeV^{-1}} \tag{8}$$

with

$$A = \left(-5.8 - \frac{1.82}{(E_\mathrm{p} - m_\mathrm{p})^{0.4}} + \frac{13.5}{(E_{\pi^0} - m_{\pi^0})^{0.2}} - \frac{4.5}{(E_{\pi^0} - m_{\pi^0})^{0.4}}\right).$$

Both parameterizations were integrated and compared with experimental results up to ~50 GeV in Blattnig et al.'s (2000) paper. It was found that a single expression is needed to represent the total inclusive cross section,

$$\sigma_{\pi^0}(E_\mathrm{p}) = \left(0.007 + 0.1\frac{\ln(E_\mathrm{p} - m_\mathrm{p})}{(E_\mathrm{p} - m_\mathrm{p})} + \frac{0.3}{(E_\mathrm{p} - m_\mathrm{p})^2}\right)^{-1} \mathrm{mb}, \tag{9}$$

where rest masses and energies must be given in units of GeV. These two differential cross section parameterizations proposed by Blattnig et al. are not deprived of problems if extrapolated to high energy. The parameterization of the Stephen and Badhwar's model grossly underpredicts the highest energy pion yield, whereas the newest Blattnig et al. (Eq. (8)) overpredicts it. The γ-ray photon yield that is output from the use of these two differential cross sections in Eqs. (4) and (5) is also shown for an Earth-like spectrum, in Fig. 11.

However, the inclusive total inelastic cross section (9) seems to work well at energies higher than 50 GeV, which we show in Fig. 12, together with a compilation of experimental data (Dermer 1986b). In the same figure we also show the results for the inclusive total cross section from model A of Kamae et al. (2005), obtained from his Fig. 5. Indeed, this model produces a slightly higher cross section, although both correlate reasonably well with experimental data, at least up to 3 TeV[5]. It is the differential cross section parameterization

[5] This figure enlarges the comparison of the Blattnig et al. (2000) inclusive cross section with experimental data (see their Fig. 4), where only three low-energy data points from Whitmore (1974) were considered.

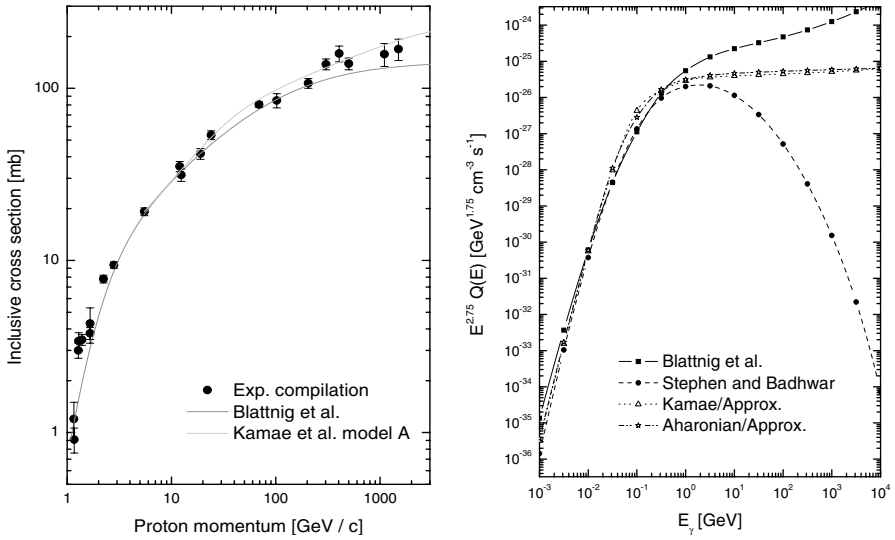

Fig. 12. *Left*: comparing inclusive cross sections. Kamae et al.'s model A data comes from their Fig. 5. The Blattnig et al. curve is obtained from Eq. (9) and the experimental compilation is from Dermer (1986b). *Right*: γ-ray emissivities as in Fig. 11 multiplied by $E^{2.75}$, with 2.75 being the slope of the proton primary spectrum.

Table 4. Integrated emissivities for an Earth-like spectrum. Values are in units of photons cm^{-3} s^{-1}.

Parameterization/Approx.	$E > 100$ Mev	$E > 100$ GeV	$E > 315$ GeV
Blattnig et al.	3.2E-25	2.2E-28	4.7E-29
Kamae et al.	4.8E-25	1.8E-29	2.6E-30
Aharonian	4.0E-25	2.2E-29	3.1E-30
Stephen and Badwhar (from Blattnig et al.)	2.2E-25	1.8E-31	1.9E-33

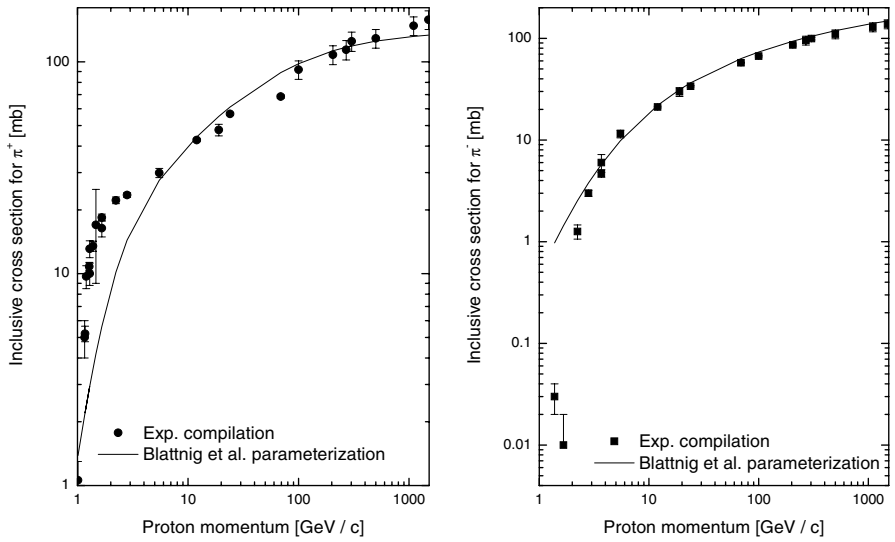

Fig. 13. Comparing inclusive cross sections for charged pions. Solid curves are obtained from Eqs. (30) and (31) of Blattnig et al. (2000b), and experimental compilation is from Dermer (1986b).

(given by Eq. (8)) that looks suspicious at such high energies. The right panel of Fig. 12 shows the emissivities as computed in the different approaches multiplied by $E^{2.75}$. As expected, Stephen and Badhwar's parameterization falls quickly at high energy, whereas both the Kamae et al. and Aharonian and Atoyan cross sections ensure that the γ-rays emitted maintain a spectrum close to that of the proton primaries. For γ-rays above few TeV (i.e., γ-rays mostly generated by protons above few tens of TeV), Blattnig et al. differential cross section parameterization makes the γ-ray emitted spectrum much harder than the proton spectrum that produced them. This signals that a direct extrapolation of Eq. (8) for computing photon emissivity above TeV with Eq. (5) induces overpredictions of fluxes.

Table 4 presents the results for the integrated emissivity, $\int_E Q(E)\,\mathrm{d}E$, with $Q(E)$ being the different curves of Fig. 11. To obtain integrated fluxes from a source of volume V at a distance D, one has to multiply by the constant $V/(4\pi D^2)$, so that the difference in integrated emissivities indeed represent those among integrated fluxes. As Table 4 shows –disregarding those coming from the Blattnig et al. parameterization of Stephen and Badwhar's results, which are quoted here just for completeness – above 100 MeV, differences are less than a factor of 1.5, which most likely is washed away by other uncertainties in any given model. But above 300 GeV, difference are larger and a conservative choice is in order.

If interested in the GLAST-domain (say, $E > 100$ MeV, $E < 50$ GeV) predictions, the most conservative choice seems to be to use the new Blattnig et al. differential cross section parameterization (Eq. (8)), with no other approximation, in Eqs. (4) and (5). This choice, while not taking non-diffractive processes into account, will possibly *slightly underpredict* the integrated flux (as shown in Table 4). Up to this moment, there is no public parameterization of the differential cross section including diffractive effects, but one is to be presented soon (T. Kamae, private communication). By using the Blattnig et al. approach, there is no δ-function approximation involved or an ad-hoc histogram of particle numbers as proposed in the treatment of Kamae et al. (2005). One has an analytical expression that can be directly used in the numerical estimates of Eq. (5). However, the price to pay is that this form of computation cannot be considered reliable at higher energies and should not be used.

For the IACTs-domain ($E > 100$ GeV), the safest and also computationally-preferable choice appears to be to take either Kamae et al.'s model A, or even the simpler Aharonian and Atoyan's expression (Eq. (7)) and a δ-function approximation. This approach would probably be slightly underestimating the integrated flux at such high energies. All in all, assuming either Kamae et al.'s or Aharonian and Atoyan's expression for all energies does not introduce substantial differences, as Table 4 shows.

Finally, in Fig. 13 we compare the inclusive cross sections for charged pions with experimental data up to about 1 TeV, which are again found to agree with experimental data, except for a bunch of data points at low proton energies in the case of positive charged pions. In any case, for situations where the density of cosmic rays or of target nuclei or both are high, neutral pion decay is expected to be the dominant process above 100 MeV, so that possible uncertainties in parameterizations of the cross sections of charged pions are not expected to play a significant role in the prediction of fluxes.